2-3-2004

Dedicated polarimeter design for hard x-ray and soft gamma-ray astronomy

Mark L. McConnell
University of New Hampshire - Main Campus, mark.mcconnell@unh.edu

J Ledoux
University of New Hampshire - Main Campus

John R. Macri
University of New Hampshire - Main Campus, John.Macri@unh.edu

James M. Ryan
University of New Hampshire, James.Ryan@unh.edu

Recommended Citation

Mark L. McConnell ; James Ledoux ; John Macri and James Ryan "Dedicated polarimeter design for hard x-ray and soft gamma-ray astronomy", Proc. SPIE 5165, X-Ray and Gamma-Ray Instrumentation for Astronomy XIII, 334 (February 3, 2004); doi:10.1117/12.505713; http://dx.doi.org/10.1117/12.505713

Dedicated polarimeter design for hard x-ray and soft gamma-ray astronomy

M.L. McConnell[1], J. Ledoux, J. Macri, J. Ryan
Space Science Center, University of New Hampshire, Durham, NH 03824

ABSTRACT

We have developed a modular design for a hard X-ray and soft gamma-ray polrimeter that we call GRAPE (Gamma RAy Polarimeter Experiment). Optimized for the energy range of 50-300 keV, the GRAPE design is a Compton polarimeter based on the use of an array of plastic scintillator scattering elements in conjunction with a centrally positioned high-Z calorimeter detector. Here we shall review the results from a laboratory model of the baseline GRAPE design. The baseline design uses a 5-inch diameter position sensitive PMT (PSPMT) for readout of the plastic scintillator array and a small array of CsI detectors for measurement of the scattered photon. An improved design, based on the use of large area multi-anode PMTs (MAPMTs), is also discussed along with plans for laboratory testing of a prototype. An array of GRAPE modules could be used as the basis for a dedicated science mission, either on a long duration balloon or on an orbital mission. With a large effective FoV, a non-imaging GRAPE mission would be ideal for studying polarization in transient sources (gamma ray bursts and solar flares). It may also prove useful for studying periodically varying sources, such as pulsars. An imaging system would improve the sensitivity of the polarization measurements for transient and periodic sources and may also permit the measurement of polarization in steady-state sources.

Keywords: X-ray, X-ray astronomy, gamma-ray, gamma-ray astronomy, polarimetry, polarization, gamma-ray burst, solar flare

1. INTRODUCTION

Many emission processes that can generate hard X-ray photons can also result in the linear polarization of those hard X-ray photons.[1] The level of polarization, however, may depend on the precise emission geometry. In addition, the energy-dependence of the polarization can provide clues to the emission mechanisms that may be operating. Polarization measurements therefore have the potential to tell us something about both the mechanisms and source geometries responsible for the observed emissions. At least four emission mechanisms can lead to linearly polarized emissions at hard X-ray energies: 1) the various types of magnetobremsstrahlung radiations (cyclotron, synchrotron and curvature radiation) are all potential sources of linearly polarized emission, depending on the magnetic field configuration; 2) electron-proton bremsstrahlung emission can produce levels of linear polarization of up to 80%; 3) initially unpolarized photons can be polarized by Compton scattering, the very same process by which we produce polarized photons in the laboratory; and 4) magnetic photon splitting $\gamma \rightarrow \gamma\gamma$ can lead to polarization levels of up to 30%. Below we outline some specific scenarios for producing linearly polarized hard X-ray and γ-ray emissions.

1.1 Gamma-Ray Bursts

In recent years, largely as a result of the observation of several X-ray, optical and radio afterglows, there has developed a growing consensus that classical γ-ray bursts (GRBs) are at cosmological distances. Such great distances imply that a typical GRB releases $10^{51} - 10^{53}$ ergs or more within a time span of several seconds. The general picture that has emerged is one that describes the GRB phenomenom in terms of a relativistic fireball model.[2,3] According to this scheme, the γ-rays are emitted when an ultra-relativistic energy flow is converted into radiation. The nature of the "inner engine,, that releases this energy flow is still a subject of speculation. Once released, however, it is believed that the prompt gamma-ray emission is produced by internal shocks within the outgoing flow. Internal shocks are generated when one expanding shell overtakes another, slower-moving shell. An external shock arises when the outgoing flow runs into the local interstellar medium (ISM). The longer wavelength (soft X-ray, optical, radio) afterglow emission is believed to arise from the external shock.

[1] e-mail: Mark.McConnell@unh.edu

X-Ray and Gamma-Ray Instrumentation for Astronomy XIII, edited by Kathryn A. Flanagan, Oswald H. W. Siegmund, Proceedings of SPIE Vol. 5165 (SPIE, Bellingham, WA, 2004)
0277-786X/04/$15 · doi: 10.1117/12.505713

A common feature of many GRB models is that the energy release takes the form of jets that are directed along the rotation axis of the system. Several indirect arguments have been used to argue that such jets are required to explain the observations. For example, a break in the afterglow light curve from a relatively shallow power-law decay to a steeper exponential decay can be interpreted as a result of a beam that is laterally expanding with time.[4-6] *Since the energy budget of a given GRB depends heavily on assumptions about the extent to which the flow is jet-like, determining the reality and nature of jets in GRBs is becoming an important goal of future observations.*

The observation of optical polarization (up to ~10%) in several GRB afterglows[7-9] has provided *direct* evidence for geometrical beaming of emission related to the external shocks. Several models predict levels of polarization as high as 10 or 20%, depending on the angle between the observer and the jet axis.[10-13] These optical studies, however, probe only the external shock region. *In the context of the canonical fireball model, measurements of the hard X-ray polarization during the prompt phase of the GRB promise to provide a similar probe of the internal shock region.* Since the outgoing flow at the internal shock is expected to be more tightly collimated than the flow at the external shock (resulting from a continuous spreading of the jet as it progresses outward through the fireball), one can expect a somewhat higher level of hard X-ray polarization (assuming that it arises from synchrotron emission) during the prompt phase of the GRB. Even higher levels of polarization might be expected if the emission results from inverse Compton, rather than synchrotron, emission. For example, one model[14] proposed that the γ-radiation is generated by Compton scattering off relativistic electrons in the (inner) transient jet, not unlike models proposed for AGN.[15] In this model, significant levels of polarization of the hard X-ray emission (>20%) are predicted for all bursts with durations between 1 and 30 seconds. Even moderate sensitivity to polarization (20-30%) will help to constrain some of the models. The recent claim[16] of a very high level of polarization (80%) at energies between 150 keV and 2 MeV underscores the potential for hard X-ray polarization measurements of GRBs. Although there is as yet no consensus on the precise implications of such a high polarization level, it is clear that magnetic fields must play a crucial role in the GRB explosion.

The low energy part of the GRB spectrum, which behaves as a power-law, suggests an origin due to synchrotron emission from relativistic electrons, but a simple synchrotron model cannot explain the entire spectrum.[2] Models for the GRB spectrum typically involve both synchrotron and/or inverse Compton emission.[14,17] Both mechanisms can lead to significant polarization, but with different energy-dependences. The uncertainty with regards to the origin of the hard X-ray spectrum is a problem that can also be attacked, at a fundamental level, using polarization measurements. Both inverse Compton and synchrotron emission have been proposed as viable emission mechanisms for GRBs. The spectral signatures of these two processes can be very similar, so it is very difficult to determine the responsible mechanism on the basis of spectral measurements alone. Energy-dependent polarization measurements, in principle, offer a possible solution. The degree of linear polarization of synchrotron emission, unlike inverse Compton emission, is independent of energy. *This energy-dependence of the polarization (or lack thereof) may therefore be exploited as a means of identifying the emission mechanism responsible for the hard X-ray and γ-ray emission.*

It is widely recognized that the soft γ-ray repeaters (SGR) represent a different class of phenomena than the classical GRBs. SGRs are short duration, soft-spectrum bursts with super-Eddington luminosities. The bulk of the emission is seen at energies below 100 keV. A total of four, perhaps five, such sources have now been identified.[18] The prevailing view is that SGR outbursts involve emission from the vicinity of magnetars, neutron stars with magnetic fields in excess of 10^{14} G, with the energy release triggered by massive neutron star crustquakes.[19] It has been suggested[20] that the softness of the events can be attributed to photon splitting ($\gamma \rightarrow \gamma\gamma$) in the extremely intense magnetic fields. The photon splitting process degrades the high energy γ-ray photons to hard X-ray energies.[21] One by-product of photon splitting is that the reprocessed photons would exhibit a polarization level of ~25%.[20] *Polarization measurements of the 50–300 keV could therefore provide a test of the importance of photon splitting in SGRs.*

1.2 Solar Flares

The study of polarization from solar flares at hard X-ray energies is especially appealing in that the hard X-ray emission from any bremsstrahlung source (such as a solar flare) will be polarized if the phase-space distribution of the emitting electrons is anisotropic. *Polarization measurements therefore provide a direct handle on the extent to which the accelerated electrons are beamed, which, in turn, has important implications for particle acceleration models.* Studies of γ-ray line data from the SMM Gamma Ray Spectrometer (GRS) suggest that protons and α-particles are likely being accelerated in a rather broad angular distribution.[22,23] There is no reason to expect, however, that electrons are being accelerated in a similar fashion.

The first measurements of X-ray polarization from solar flares (at energies of ~15 keV) were made by Soviet experimenters using polarimeters aboard the Intercosmos satellites. In their initial study, they reported[24] an average

polarization for three small X-ray flares of P = 40(±20)%. This study was followed by an analysis[25,26] of three flares in October and November of 1970 that showed polarizations of approximately 20% during the hard impulsive phase. These reports were met with considerable skepticism, on the grounds that they did not adequately allow for detector cross-calibration issues and limited photon statistics.[27] Subsequent observations with an instrument on the OSO-7 satellite seemed to confirm the existence and magnitudes of the polarizations (~10%), but these data were compromised by in-flight gain shifts.[28] In a later study[29] using a polarimeter on Intercosmos 11, polarizations of only a few percent were measured at ~15 keV for two flares in July 1974. This small but finite polarization is consistent with the predictions for purely thermal emission that contains an admixture of polarized backscattered radiation.[30] A small polarimeter was flown on an early shuttle flight (STS-3) and made measurements of eight C- and M-class flares in the 5–20 keV energy range. Upper limits in the range of 2.5% to 12.7% were measured, although contamination of the Li scattering material invalidated the pre-flight calibration.[31]

The most recent effort to measure hard X-ray polarization from solar flares comes from the Ramaty High Energy Solar Spectroscopic Imager (RHESSI).[32,33] Although designed primarily as a hard X-ray imager and spectrometer, the Ramaty High Energy Solar Spectroscopic Imager (RHESSI) is also capable of measuring the polarization of hard X-rays (20–100 keV) from solar flares.[34,35] This capability arises from the inclusion of a small unobstructed Be scattering element that is strategically located within the cryostat that houses the array of nine germanium detectors. The Ge detectors are segmented, with both a front and rear active volume. Low energy photons (below about 100 keV) can reach a rear segment of a Ge detector only indirectly, by scattering. Low energy photons from the Sun have a direct path to the Be and have a high probability of Compton scattering into a rear segment of a Ge detector. The azimuthal distribution of these scattered photons carries with it a signature of the linear polarization of the incident flux. Sensitivity estimates, based on Monte Carlo simulations and in-flight background measurements, indicated that a 20–100 keV polarization sensitivity of less than a few percent could be achieved for X-class flares. Data from the X4.3 flare of 23-July-2003 has recently provided evidence for 20-40 keV polarization at a level of ~27% from the 23-Jul-2002 solar flare.[34-36] However, it is not yet clear whether this modulation results from the linear polarization of the incident flux or from residual systematic effects.[35] In principle, the capability of RHESSI to simultaneously image the hard X-ray emission represents a major advantage over previous efforts to measure hard X-ray polarization, in that photospherically backscattered photons may be directly imaged by RHESSI as a constraint on the contribution of such backscattered photons to the primary signal.

1.3 Other Sources

Several other hard X-ray sources may also represent interesting targets for polarization studies.[37] Here we review some of those sources that may be detectable by a balloon borne GRAPE observation. Of particular interest will be observations of the Crab Nebula. Observations indicate a polarization fraction that increases with energy, from 8.1% at optical wavelengths[38] to 19% at soft X-ray energies.[39] The consistency in the polarization angle in these data suggests that a single mechanism, most likely synchrotron radiation, is responsible for the emission. A similar measurement at higher energies would help determine the extent to which the high-energy emission is related to that at longer wavelengths.

Accreting black hole sources (both AGN and stellar mass black holes) also present an opportunity for useful polarization studies. Data from OSO-8 provided evidence[40] for small levels of polarization (2-5%) at low energies (<10 keV) from Cyg X-1, but these observations have never been confirmed. Linear polarization is expected from low-energy photons scattering off hot electrons in an accretion disk.[41] The degree of polarization depends on the angle of emission with respect to the disk and the optical depth of the emission region. For optically thin disks, polarization levels as high as 30-60% are possible. For structured accretion disks, energy-dependent polarization studies may permit us to probe the details of that structure. Beamed radiation from accreting black hole sources is also a possible source of polarization (for some of the same reasons that we expect polarization from GRBs). Beams in AGN, for example, are highly polarized at optical and radio wavelengths, most likely due to synchrotron emission. One model[15] of the hard X-ray emission from Cen A redicted high levels of polarization (~60%) up to ~300 keV. Similar models could be considered for many of the so-called "X-ray novae,, (especially those that exhibit jet features). Some of these sources can occasionally reach intensities that are comparable to the Crab, at which time they would make excellent candidates for polarization studies.

2. THEORY OF COMPTON SCATTER POLARIMETERS

The basic physical process used to measure polarization in the 50-300 keV energy range is Compton scattering. The Compton scattering cross section (as given by the Klein-Nishina formula) is determined by the frequency (ν_O) of the incident photon, the *scattering angle* (θ) of the scattered photon measured from the direction of the incident photon, and the *azimuthal angle* (η) of the scattered photon measured from the plane containing the electric vector of the incident photon. For a given value of θ, the scattering cross section for polarized radiation reaches a minimum at $\eta = 0°$ and a maximum at $\eta = 90°$. In other words, photons tend to be scattered at a right angle with respect to the incident electric field. In the case of an unpolarized beam of incident photons, there will be no net positive electric field vector and therefore no preferred azimuthal scattering angle (η); the distribution of scattered photons with respect to η will be uniform. However, in the polarized case, the incident photons will exhibit a net positive electric field vector and the distribution in η will be asymmetric. The magnitude of the asymmetry is largest at low energies (below 100 keV) and is most pronounced for scatter angles near $\theta = 90°$.

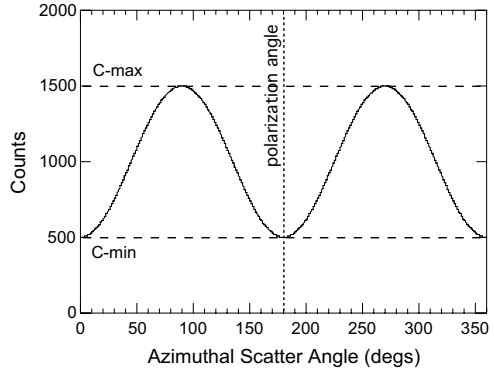

Figure 1: The modulation pattern produced by Compton scattering of polarized radiation. The minimum of the modulation pattern defines the plane of polarization of the incident flux.

In general, a Compton scatter polarimeter consists of two detectors to determine the energies of both the scattered photon and the scattered electron. One detector, the *scattering detector*, provides the medium for the Compton interaction to take place. Ideally, this detector is designed to maximize the probability of there being a single Compton interaction with a subsequent escape of the scattered photon. This requires a low-Z material in order to minimize photoelectric interactions. The primary purpose of the second detector, the *calorimeter*, is to absorb the full energy of the scattered photon. In principle, one can use the same material for both the scattering elements and the calorimeter elements, in which case the lower limit of the operational energy band is approximately defined by the transition from the Compton to the photoelectric regime of the detection material.[1] For example, the optimized lower limits for plastic, CsI, and CZT are ~100 keV, ~200 keV and ~300 keV, respectively. *Energy thresholds near 50-100 keV can best be achieved using low-Z plastic scintillator as a scattering element in conjunction with a high-Z calorimeter.*[1,42,43] Since the energy loss is dominated by that of the calorimeter, the total energy resolution of the polarimeter is determined largely by that of the calorimeter.

The accuracy with which the scattering geometry can be measured helps determine the ability to define the modulation pattern (Fig. 1). This capability has a direct impact on the polarization sensitivity, since the ultimate goal of a Compton scatter polarimeter is to measure the azimuthal modulation pattern of the scattered photons. The integrated azimuthal distribution of the scattered photons is given by,

$$C(\eta) \;=\; A\cos\left(2\left(\eta-\varphi+\frac{\pi}{2}\right)\right) \;+\; B \qquad (1)$$

where φ is the polarization angle of the incident photons; A and B are constants used to fit the modulation pattern (c.f., Figure 1). The quality of the polarization signal is quantified by the *polarization modulation factor*.[1,44] For a given energy and incidence angle for an incoming photon beam, this can be expressed as,

$$\mu_p \;=\; \frac{C_{p,\max}-C_{p,\min}}{C_{p,\max}+C_{p,\min}} \;=\; \frac{A_p}{B_p} \qquad (2)$$

where $C_{p,max}$ and $C_{p,min}$ refer to the maximum and minimum number of counts registered in the polarimeter, respectively, with respect to η; A_p and B_p refer to the corresponding parameters in equation (1). In this case the 'p' subscript denotes that this refers to the measurement of a beam with unknown polarization. In order to determine the polarization of the measured beam, we need first to know how the polarimeter would respond to a similar beam, but with 100% polarization (μ_{100}). This can be done using Monte Carlo simulations. Then we can then use this result, in conjunction with the observed modulation factor (μ_P), to determine the level of polarization in a measured beam,

$$P = \frac{\mu_p}{\mu_{100}} \tag{3}$$

where P is the measured polarization. The minimum detectable polarization (MDP) can be expressed as,

$$MDP(\%) = \frac{n_\sigma}{\mu_{100}\, R_{src}} \sqrt{\frac{2\,(R_{src} + R_{bgd})}{T}} \tag{4}$$

where n_σ is the significance level (number of sigma), R_{src} is the total source counting rate, R_{bgd} is the total background counting rate and T is the total observation time. Improved sensitivity to source polarization can be achieved either by increasing the modulation factor (μ_{100}) or by increasing the effective area of the polarimeter (thereby increasing the source counting rate, R_{src}).

3. GRAPE DEVELOPMENT STATUS

We have been working on the development of hard X-ray polarimeters (50-300 keV) for several years. Our initial paper[45] discussed a simple polarimeter design consisting of a ring of twelve individual scattering detectors (composed of low-Z plastic scintillator) surrounding a single NaI calorimeter. A prototype of this simple design was tested in the laboratory, in part to validate the Monte Carlo code.[46,47] Since that time, our designs have evolved considerably, although the essential concept remains unchanged. Our designs have focused on two principal means of optimizing the performance of a Compton scatter polarimeter: 1) by more precisely measuring the scattering geometry of each event; and 2) by rejecting those events that undergo multiple Compton scattering within the scattering elements. A better geometry definition will serve to more clearly define the modulation pattern of the incident flux. Improved rejection of multiple scatter events will reduce the contribution of such events to the unmodulated component of the polarization response.

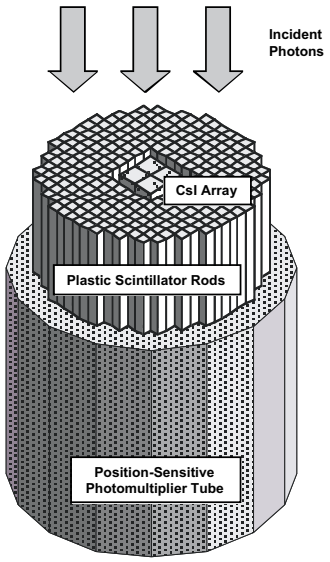

Figure 2: The original GRAPE design showing the layout of the plastic scintillator elements and CsI(Na) elements on the front surface of a PSPMT. Not shown here is the 4-element multianode PMT used for readout of the CsI(Na) array.

3.1 GRAPE Science Model 1 – A PSPMT-Based Design

We developed a modular polarimeter design that places an entire device on the front end of a single 5" diameter position-sensitive PMT (PSPMT).[46-48] The design, shown in Fig. 2, incorporates an array of plastic scintillator elements to provide the necessary spatial resolution in the scattering medium and to allow for the rejection of multiple scatter events. Each plastic scintillator element is optically isolated with a cross sectional area of 5 × 5 mm^2. The plastic elements are arranged in the form of an annulus having an outside diameter of 10 cm (corresponding to the sensitive area of the Hamamatsu R3292 5" PSPMT). The central portion of the annulus is large enough to accomodate a 2 × 2 array of 1 cm CsI(Na) scintillators. The CsI(Na) scintillators are coupled to their own independent multi-anode PMT (Hamamatsu R5900 MAPMT) for the energy measurement and coincidence timing. An ideal event is one in which the incident photon Compton scatters in one plastic element and is subsequently absorbed in one element of the central CsI array.

Monte Carlo simulations were used to characterize this design. The small cross-sectional area of each scintillator element ensures that practically all multiple-scatter events are identified. The lower energy threshold, particularly in the scattering elements, has a significant influence on the performance of the polarimeter at low energies. For the simulations, we have assumed a threshold of 10 keV in the plastic scintillator and 15 keV in the CsI scintillators. The simulation results are shown in Fig. 3 for the case of a vertically-incident flux on a single GRAPE module with various detector depths. As one might expect, the effective area (εA) increases with increasing detector depth. (In practice, the advantage of an increased effective area for a deeper detector must also be offset by the decrease in light collection efficiency, an effect that is not considered here.) The modulation factor (μ_{100}) can be combined with the effective area to define a figure-of-merit (FoM). The FoM also takes into account the effect of detector background, which we assume scales as the volume of the detector (V_{det}). In particular, the FoM is defined (under the assumption of a background-dominated measurement) as,

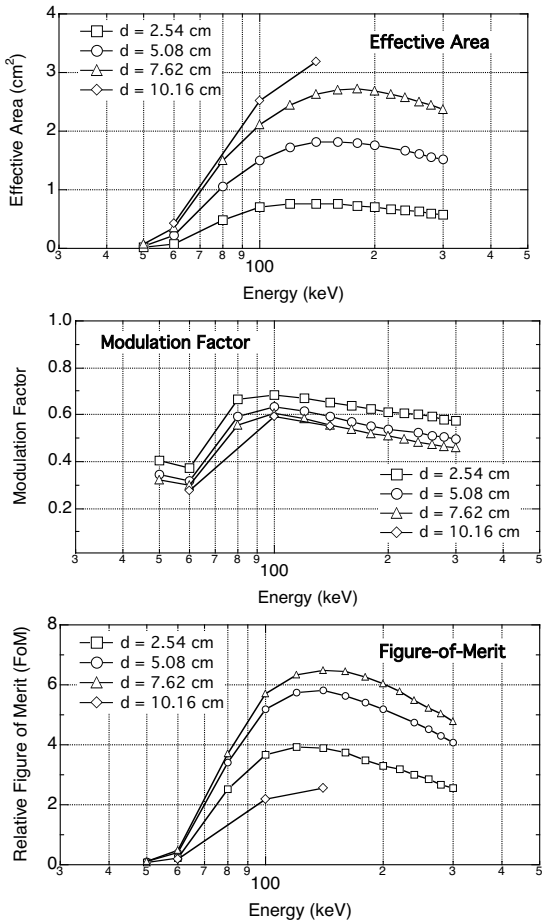

Figure 3: The effective area, modulation factor and figure-of-merit of the PSPMT-based GRAPE design as a function of energy for various detector depths (d).

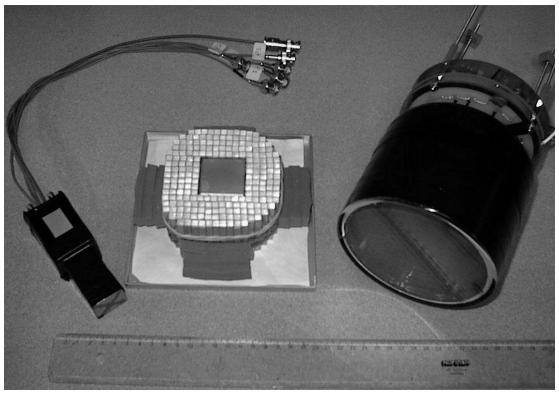

Figure 4: Components of GRAPE science model 1 (SM1), showing the calorimeter assembly (left), the plastic scintillator array (middle) and the 5-inch PSPMT (right).

$$FoM = \frac{\mu_{100}\,\varepsilon A}{\sqrt{V_{\text{det}}}} \qquad (5)$$

From the FoM we see that the effectiveness of this design peaks in the 100–200 keV energy band. These data also indicate that a depth of ~5–7 cm is near-optimum, a value that represents a compromise between efficiency and the volume-dependent background.

One very useful aspect of the GRAPE design is that there exists a significant polarization response at large incidence angles.[49] Since the exposed geometric area of the detector remains relatively constant, the effective area remains relatively constant out to fairly large angles. Although there is a significant decrease in the modulation factor at large angles, there is still significant polarization response even at 60° incidence angle. The off-axis response of this design would be very useful in studies of GRBs, where a large FoV represents a distinct advantage.

3.2 Development of Science Model 1 (SM1)

We have recently completed testing a GRAPE science model (SM1), based on the design depicted in Fig. 2.[49-53] The plastic scintillator array is composed of 250 individual pieces of Bicron BC-404 scintillator. Each 5 mm × 5 mm × 50 mm scintillator element is individually wrapped in Tyvek® to maximize light collection efficiency and to provide optical isolation. A thin layer of Kapton® tape was then used to hold the wrapping in place. A thin aluminum housing encloses both the PSPMT and the plastic scintillator array. The calorimeter detector assembly is a 2 × 2 array of 1 cm × 1 cm × 5 cm CsI(Na) elements coupled to a MAPMT (Hamamatsu R5900 with a 2 × 2 anode array) and enclosed within its own, separate light-tight housing. Fig. 4 shows the major components of the device. During operations, the calorimeter detector assembly is inserted into a central well in the PSPMT / plastic scintillator housing. The configuration makes use of a charge division network for readout of the PSPMT (Hammamatsu R3292) that provides a weighted average of the spatial distribution of the measured light output using only four signals (two signals in x and 2 signals in y). The readout electronics, including a preamplifier for each of the four readout signals, are included in the Hamamatsu assembly.

A source of polarized photons was generated by Compton scattering photons from a radioactive source.[47,54] The level of polarization of such a scattered photon beam is dependent on both the initial photon energy and the photon scatter angle.[47,55] The scattering of photons from a ^{137}Cs source, for example, generates 288 keV photons with a polarization fraction of ~55–60%. The use of plastic scintillator as a scattering block to generate the polarized beam permits the electronic tagging of the scattered (polarized) photons.

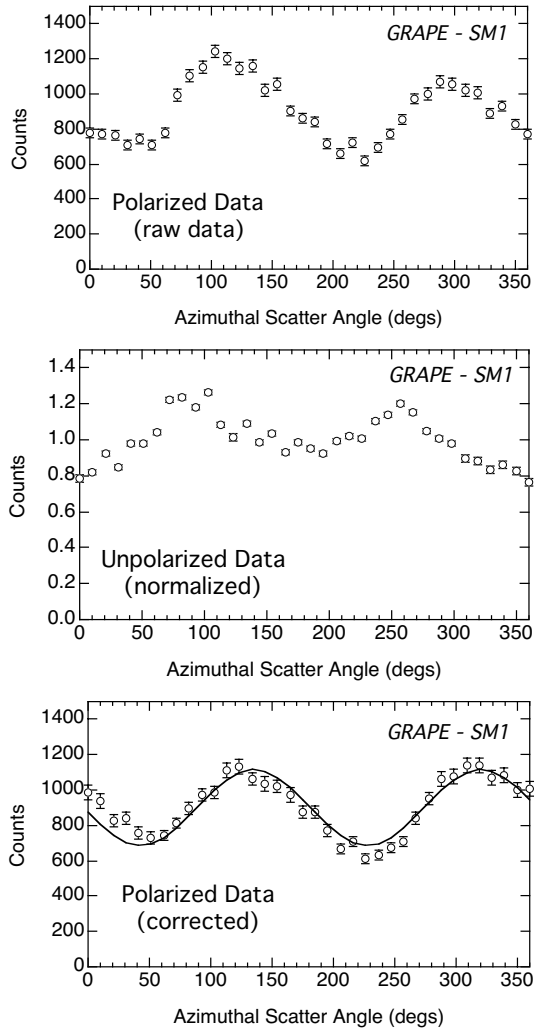

Figure 5: Lab data from SM1 showing how the measured data is corrected for intrinsic geometric effects to extract the true modulation pattern (see text).

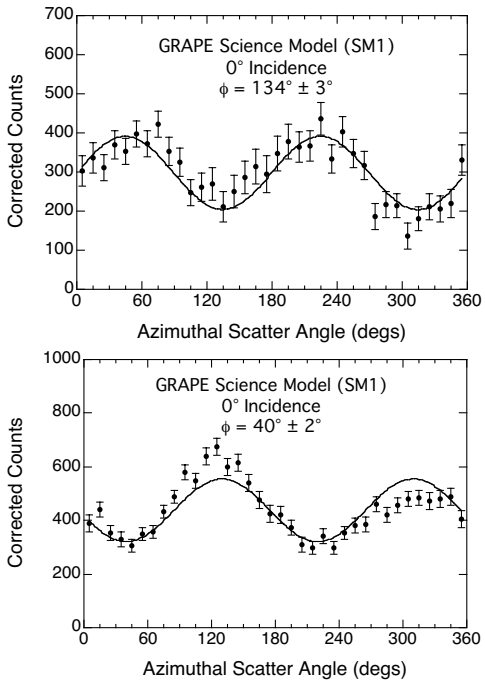

Figure 6: Lab data from SM1 showing the response at two different polarization angles (differing by ~90°).

Fig. 5 illustrates the nature of the GRAPE SM1 laboratory data. The first panel shows the polarization response to a partially polarized monoenergetic beam of ~288 keV photons (generated by scattering photons from ^{137}Cs) vertically incident on the front surface of the polarimeter. This distribution includes not only the intrinsic modulation pattern due to the Compton scattering process, but it also includes geometric effects related to the specific layout of the detector elements within the polarimeter and the associated quantization of possible scatter angles. The geometric effects can be more clearly seen in the case of an incident beam that is completely unpolarized (direct photons from a ^{133}Ba calibration source), as shown (normalized to an average value of 1.0) in the second panel of Fig. 5. (In practice, for analyzing real data, this unpolarized distribution would be determined by simulations rather than by direct measurements.) To extract the true distribution of polarized events, we divide the polarized distribution by the (normalized) unpolarized distribution. Only when we correct the raw data in this fashion do we clearly see the cos 2η modulation pattern that is expected (the third panel of Fig. 5). In this case, the measured level of polarization (based on the measured modulation and that expected for a completely polarized beam) is 55(±2)%, in very good agreement with the value of 55-60% that we expect for scattered ^{137}Cs photons. Fig. 6 shows lab data collected for two different polarization angles of the incident beam ($\Delta\phi \approx 90°$); a corresponding shift in the phase of the modulation pattern is clearly seen.

We have completed a series of calibration runs to more fully document the characteristics of SM1 as a function of incidence angle. This includes runs with both polarized and unpolarized photon beams, along with background measurements. We are currently working on the final analysis of these data.

3.3 GRAPE Science Model 2- An MAPMT Design

We have recently assembled a second science model (SM2) based on a new design that builds on our success with SM1. This design incorporates the new large-area flat-panel MAPMT from Hamamatsu (H8500), that provides an 8 × 8

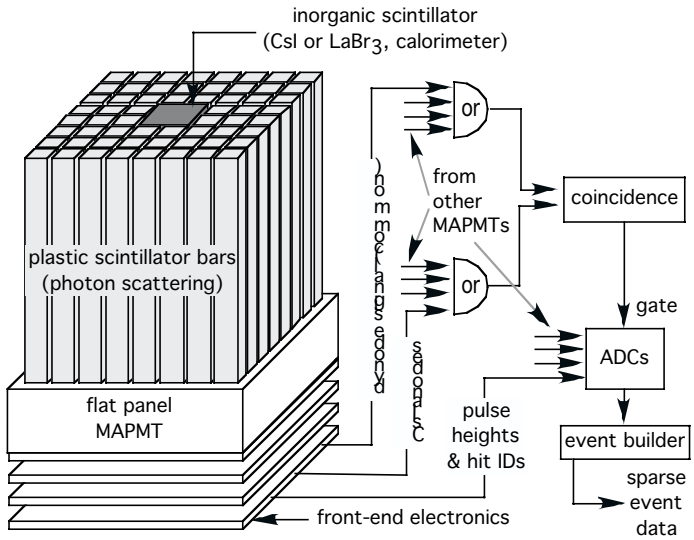

Figure 7: Diagram of SM2, showing the layout of the scintillator components and the general scheme for signal processing and handling.

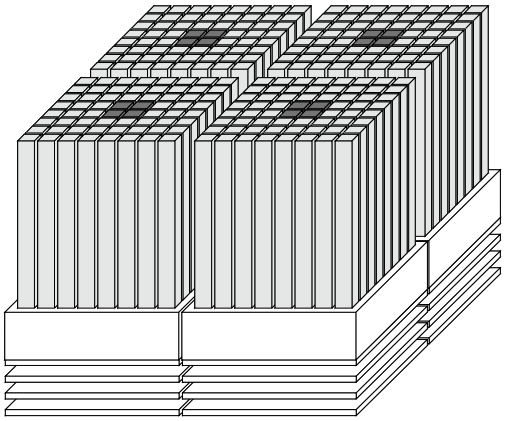

Figure 8: Diagram showing the tiling of four SM2-type GRAPE modules, shown here with segmented calorimeters.

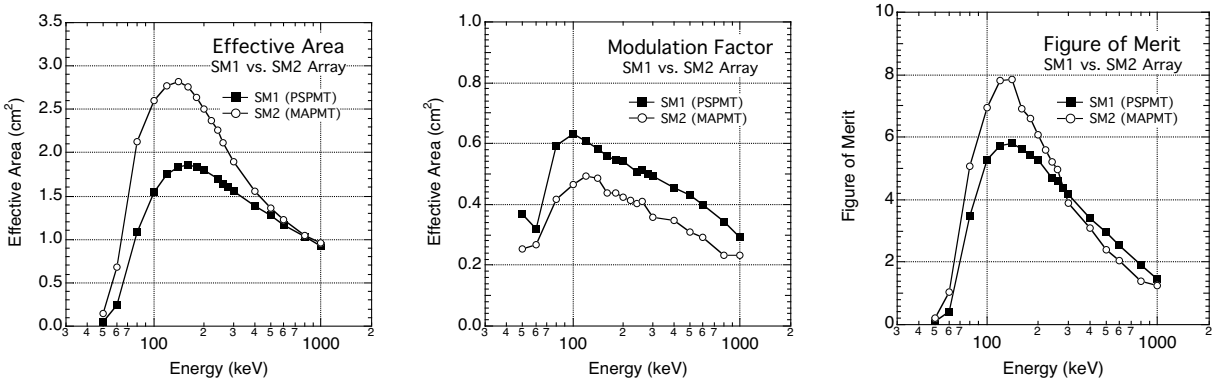

Figure 9: Simulated characteristics of the SM1 design versus a 4-element array of SM2 modules. The geometric area of the SM2 array is ~30% smaller than the single SM1 module.

array of independent anodes on a single device measuring 52 mm × 52 mm in area and 28 mm in depth. The pitch of the anode array (6 mm) is an excellent match to the 5 mm size of the plastic scintillating elements that we are currently using. (A 264-channel version with 3 mm pitch is currently under development by Hamamatsu.) As depicted in Fig. 7, the conceptual design of this detector includes a single 1 cm × 1 cm CsI(Na) crystal surrounded by an array of 60 plastic scintillating elements.

The SM2 design offers several distinct advantages over the PSPMT-based design (SM1). The geometry of the flat-panel MAPMT readily permits close packing of polarimeter modules with minimal deadspace (~10%, as seen in Fig. 8). An array of four SM2-type modules would provide roughly 60% *larger* effective area than a single SM1-type module, with a footprint that is 30% *smaller* than that of SM1. The much smaller depth of the MAPMT design results in a total volume of a 4-module array that is ~75% smaller than SM1. The tiling of SM2 modules also makes it easier to include events that involve more than one module (i.e., events that scatter from the plastic scintillators of one module into the calorimeter of an adjacent module). Although not yet studied in detail, we expect that the use of these multi-module events will improve both the detection efficiency and also the modulation factor. Another important advantage of the SM2 design is that there is no need for a second readout device. In the SM1 design, a small 4-anode MAPMT is used to (independently) read out the CsI calorimeter array. This adds a second HV line and, more importantly, places additional mass (that of the MAPMT) in the front of the polarimeter. The SM2 design uses the 64 independent anodes of the flat-panel PMT to read out both the plastic and the CsI elements. The independence of the 64 anodes allows for triggering

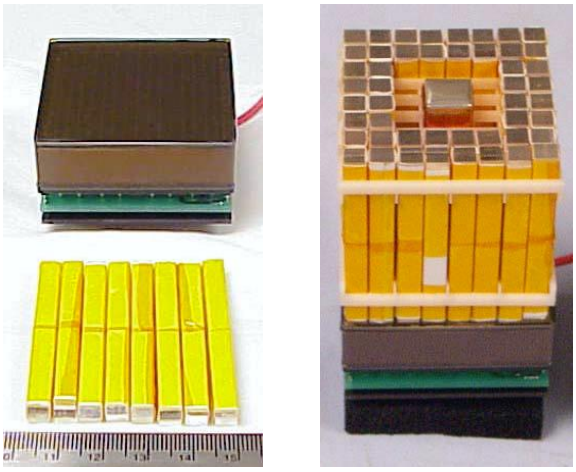

Figure 10: Assembly of SM2, showing : the flat-panel MAPMT and some of the plastic scintillator elements (left); and the plastic array assembled on top of the MAPMT (right). Note that some of the plastic elements around the central CsI have been removed for the initial tests.

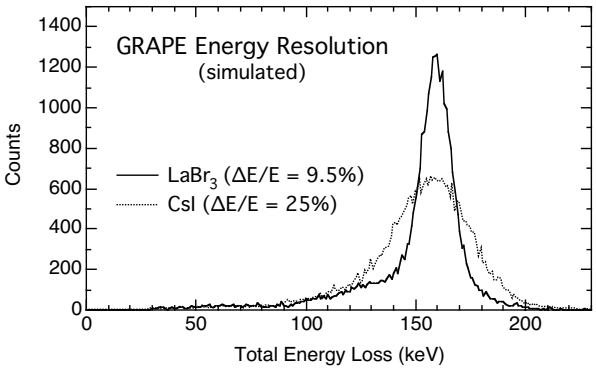

Figure 11: Simulated results showing the improved energy resolution of the SM2 design that would result from changing the CsI calorimeter to one made from $LaBr_3$.

based on having simultaneous signals in both the plastic and in the CsI. One important aspect of the SM2 testing will be the development and evaluation of trigger criteria.

A comparison of the simulated characteristics of a 2 × 2 array of SM2 modules and a single SM1 module are shown in Fig. 9. These simulations do not yet include those events that scatter from one module to another. We expect that the inclusion of these events will increase not only the effective area, but also the modulation factor of the SM2 array. So the results shown here can be considered a worst case. Nonetheless, the capabilities of the SM2 array are superior to those of a single SM1 module.

For our initial SM2 testing, we are only partially populating a single MAPMT module, as can be seen during the recent assembly of the test module (Fig. 10). This requires a minimum of electronics channels (<16) while permitting an evaluation of some of the fundamental characteristics of the design. Of particular interest, will be a demonstration of the event triggering of this configuration.

Once the initial testing of SM2 is complete, we will move on to a configuration that reads out the full set of 64 anodes. Additionally, we will replace the central CsI scintillator with one based on Lanthanum Bromide ($LaBr_3$).[56] This relatively new inorganic scintillator provides an energy resolution that is more than twice as good as NaI at 662 keV (3% vs. 7%). The timing characteristics of this new material are quite fast, with decay times (25 nsec) that are comparable to plastic scintillator. These characteristics will significantly improve the scientific capabilities of the SM2 GRAPE design. For example, the expected improvement in energy resolution, based on simulations is shown in Fig. 11.

3.4 GRAPE Source Sensitivity

In order to provide adequate sensitivity, any realistic application of the GRAPE design would involve an array of polarimeter modules. One possible deployment option for a GRAPE polarimeter array would be as the primary instrument on an Ultra-Long Duration Balloon (ULDB) payload. The ULDB technology currently under development by NASA is expected to provide balloon flight durations of up to ~100 days. A 1 m^2 array of GRAPE modules would easily fit within the envelope of a ULDB payload. The ideal configuration for GRB studies would be an array that remains pointed in the vertical direction (i.e., towards the zenith) at all times. In this case, there would be no pointing requirements, only a moderate level of aspect information (continuous knowledge of the azimuthal orientation to ~0.5°). An imaging polarimeter could also be designed to match the payload limitations of a ULDB, although the pointing requirements would be much more severe (<1° in both azimuth and zenith). A second deployment option would be as part of a spacecraft payload. This could be either a free-flying satellite or an add-on experiment for the International Space

TABLE 1
GRB Polarization Sensitivity (MDP)
(50-300 keV, ΔT = 10 sec)

Fluence (ergs cm^{-2})	*N=36 ~0.1 m^2*	*N=100 ~0.25 m^2*	*N=400 ~1 m^2*	*Observed Rate (N > Fluence)*
1×10^{-4}	9.9%	6.0%	3.0%	1 every 320 days
5×10^{-5}	14.3%	8.6%	4.3%	1 every 80 days
1×10^{-5}	35.3%	21.2%	10.6%	1 every 10 days
5×10^{-6}	55.4%	33.2%	16.6%	1 every 6 days
3×10^{-6}	79.9%	47.9%	24.0%	1 every 4 days

Station (ISS). In this case, we would be more concerned about ruggedization issues, especially with regards to the H8500 MAPMTs. If needed, smaller ruggedized MAPMTs are available (Hamamatsu R5900).

TABLE 2
Crab Polarization Sensitivity (MDP)
(50-300 keV, ΔT = 8 hours)

	Unpulsed Crab Flux			*Pulsed Crab Flux*		
E (keV)	*N=36 ~0.1 m²*	*N=100 ~0.25 m²*	*N=400 ~1 m²*	*N=36 ~0.1 m²*	*N=100 ~0.25 m²*	*N=400 ~1 m²*
50-100	6.3%	3.8%	1.9%	27.9%	16.7%	8.4%
100-150	8.9%	5.3%	2.7%	38.5%	23.1%	11.6%
150-200	15.0%	9.0%	4.5%	63.8%	38.3%	19.1%
200-250	25.6%	15.4%	7.7%	–	64.5%	32.2%
250-300	37.7%	22.6%	11.3%	–	93.4%	46.7%
300-400	44.8%	26.9%	13.4%	–	–	54.5%

To assess the capabilities of GRAPE for doing useful astrophysics, we have estimated the polarization sensitivity of a *balloon payload* based on various sized arrays of modules fabricated with flat panels MAPMTs (SM2 design). Each module is assumed to have a depth (scintillator thickness) of 5.08 cm. Somewhat thicker modules would provide improved sensitivity beyond the results shown below. We consider arrays of 36, 100, and 400 modules, representing areas of ~0.1 m^2, ~0.25 m^2, and ~1 m^2, respectively. We have used Eqn. 4 to calculate the 3σ minimum detectable polarization (MDP) of each array to both GRBs and to the Crab.

Our sensitivity calculations assume that the entire experiment is surrounded by an anticoincidence shield that effectively eliminates the background except for that which enters the open aperture. For the GRB sensitivity estimates, we assume an open aperture of π sr. For the Crab sensitivity estimates, we assume an imaging system with an 0.1 sr FoV. In both cases, we use published data[57] to estimate the magnitude of the atmospheric background flux.

The incident GRB spectrum is asumed to be represented by an $E^{-1.5}$ power law spectrum in the 50–300 keV energy band. The fluence level is defined as that integrated over the 50–300 keV energy range and we have assumed a burst duration of 10 seconds. (For a given fluence level, there is greater polarization sensitivity for the shorter events, since they involve a lower level of background.) The results of these calculations for the integrated 50-300 keV energy band are shown in Table 1. The observed rate of events is based on the fraction of events at a given fluence level in the BATSE 4B catalog[58] and the fact that BATSE observed about one event per day with its ~2π sr effective FoV. During the course of a 100-day balloon flight we could expect about ten events which provide a polarization sensitivity of better than 10% and about 25 events which provide a polarization sensitivity of better than ~30%. For the stronger events, we will be able to study the energy-dependence of the polarization. For estimating the polarization sensitivity to the Crab, we consider both the pulsed and unpulsed emission. The resulting estimates for an 8-hour exposure are shown in Table 2. Improved sensitivities would be easily achieved for a ULDB mission.

In practice, it will be important to account for the influence of systematic variations in the detector response within the polarimeter. The systematics will lead to variations in the azimuthal scatter angle distribution even in the case of an unpolarized source. One way to deal with this problem would be to map out the intrinsic systematics and use that data in the reduction of the observations. We have experience in effectively using a similar approach with a coded aperture γ-ray telescope.[59-61] It is generally believed, however, that the best approach to dealing with the systematics would be to spin the polarimeter during the observation so as to average out the influence of the various detector asymmetries. The use of both approaches may provide an effective combination. (The above sensitivity estimates assume that the systematics have been properly accounted for in the analysis.)

ACKNOWLEDGEMENTS

This work is currently supported by NASA grant NAG5-5324. We would like to thank Matt Orr for his help in the assembly of the SM2 detector.

REFERENCES

1. Lei, F., Dean, A.J., & Hills, G.L., "Compton Polarimetry in Gamma-Ray Astronomy,,, *Sp. Sci. Rev.*, **82**, 309, 1997.
2. Piran, T., "Gamma-Ray Bursts and the Fireball Model,,, *Phys. Rept.*, **314**, 575, 1999.
3. Hurley, K., Sari, R., & Djorgovski, S.G., "Cosmic Gamma-Ray Bursts, Their Afterglows and Their Host Galaxies ,,, astro-ph/0211620, 2003.
4. Rhoads, J.E., "The Dynamics and Light Curves of Beamed Gamma-Ray Burst Afterglows,,, *Ap. J.*, **525**, 737, 1999.
5. Sari, 2000

6. Panaitescu, A., & Kumar, P., "The Effect of Angular Structure of Gamma-Ray Burst Outflows on the Afterglow Emission,,, *Ap. J.*, in press, 2003.
7. Covino, S., et al., "GRB 990510: Linearly Polarized Radiation from a Fireball,,, *A&A*, **348**, L1, 1999.
8. Bersier, D., et al., "The Strongly Polarized Afterglow of GRB 020405,,, *Ap. J.*, **583**, L63, 2003.
9. Covino,. S., Ghisellini, G., Lazzati, D., & Malesani, D., "Polarization of Gamma-Ray Burst Optical and Near-Infrared Afterglows,,, astro-ph/0301608, 2003.
10. Gruzinov, A., "Strongly Polarized Optical Afterglows of Gamma-Ray Bursts,,, *Ap.J.*, **525**, L29, 1999.
11. Gruzinov, A., & Waxman, E., "Gamma-Ray Burst Afterglow: Polarization and Analytic Light Curves,,, *Ap. J.*, **511**, 852, 1999.
12. Sari, R., "Linear Polarization and Proper Motion in the Afterglow of Beamed Gamma-Ray Bursts,,, *Ap.J.*, **524**, L43, 1999.
13. Ghisellini, G., & Lazzati, D., "Polarization Light Curves and Position Angle Variation of Beamed Gamma-Ray Bursts,,, *MNRAS*, **309**, L7, 1999.
14. Shaviv, N.J., & Dar, A., "Gamma-Ray Bursts from Minijets,,, *Ap. J.*, **447**, 863, 1995.
15. Skibo, J.G., Dermer, C.D., & Kinzer, R.L., "Is the High-Energy Emission from Centaurus A Compton-Scattered Jet Radiation?,, *Ap. J.*, **426**, L23, 1994.
16. Coburn, W. & Boggs, S., "Polarization of the Prompt γ-ray Emission from the γ-Ray Burst of 6 December 2002,,, *Nature*, **423**, 415-417, 2003.
17. Pilla, R.P., & Loeb, A., "Emission Spectra from Internal Shocks in Gamma-Ray Burst Sources,,, *Ap.J.*, **494**, L167, 1998.
18. Hurley, K., "The 4.5+/-0.5 Soft Gamma Repeaters in Review,,, *The Fifth Compton Symposium,* ed. M.L. McConnell & J.M. Ryan, AIP Conf. Proc. 510, 515, AIP, New York, 2000.
19. Duncan, R., & Thompson, C., "Formation of Very Strongly Magnetized Neutron Stars - Implications for Gamma-Ray Burst,,, *Ap. J.*, **392**, L9, 1992.
20. Baring, M., "Photon-Splitting Limits to the Hardness of Emission in Strongly Magnetized Soft Gamma Repeaters,,, *Ap. J.*, **440**, L69, 1995.
21. Baring, M., "The Suppression of Pulsar and Gamma-Ray Burst Annihilation Lines by Magnetic Photon Splitting,,, *MNRAS*, **262**, 20, 1993.
22. Share, G.H., & Murphy, R.J., "Intensity and Directionality of Flare-Accelerated α-Particles at the Sun,,, *Ap. J.*, **485**, 409, 1997.
23. Share, G.H., Murphy, R.J., Kiener, J., & de Sereville, N., "Directionality of Solar Flare-accelerated Protons and α-Particles from γ-Ray Line Measurements,,, *Ap.J.*, **573**, 464, 2002.
24. Tindo, I. P., Ivanov, V. D., Mandel'stam, S. L. & Shuryghin, A. I., "On the Polarization of the Emission of X-Rays from Solar Flares,,, *Solar Physics*, **14**, 204, 1970.
25. Tindo, I. P., Ivanov, V. D., Valnicek, B. & Livshits, M. A., "Preliminary Interpretation of the Polatization Measurements Performed on 'Intercosmos-4' During Three X-Ray Solar Flares,,, *Solar Physics*, **27**, 426, 1972.
26. Tindo, I. P., Ivanov, V. D., Mandel'stam, S. L. & Shuryghin, A. I., "New Measurements of the Polarization of X-Ray Solar Flares,,, *Solar Physics*, **24**, 429, 1972.
27. Brown, J. C., McClymont, A. N. And McLean, I. S., "Interpretation of Solar Hard X-Ray Burst Polarisation Measurements,,, *Nature*, **247**, 448, 1974.
28. Nakada, M. P., Neupert, W. M. & Thomas, R. J., "Polarization Results of Solar X-Rays from OSO-7.,, *Solar Physics*, **37**, 429, 1974.
29. Tindo, I. P., Shuryghin, A. I. & Steffen, W., "The Polarization of X-Ray Emission of Some Solar Flares in July 1974,,, *Solar Physics*, **46**, 219, 1976.
30. Bai, T. & R. Ramaty, "Backscatter, Anisotropy, and Polarization of Solar Hard X-Rays,,, *Ap. J.*, **219**, 705, 1978.
31. Tramiel, L. J., Channan, G. A. & Novick, R., "Polarization Evidence for the Isotropy of Electrons Responsible for the Production of 5–20 keV X-Rays in Solar Flares,,, *Ap. J.*, **280**, 440, 1984.
32. Lin, R.P., et al., "The Reuven Ramaty High Energy Solar Spectroscopic Imager (RHESSI),,, *Solar Physics*, **210**, 3-32, 2003.
33. Smith, D.M., et al., "The RHESSI Spectrometer,,, *Solar Physics*, **210**, 33-60, 2003.
34. McConnell, M.L., Smith, D. M., Emslie, A. G., Hurford, G. J., Lin, R. P., & Ryan, J. M., "Hard X-Ray Solar Flare Polarimetry with RHESSI,,, to be published in *Energy Release and Particle Acceleration in the Solar Atmosphere - Flares and Related Phenomena*, ed. B. Dennis, R. Lin, and T. Kosugi, COSPAR Colloquia Series, Elsevier, New York, 2003.

35. McConnell, M.,L., Smith, D.M., Emslie, A.G., Hurford, G.J., Lin, R.P., & Ryan, J.M., "Measuring Hard X-Ray Polarization of Solar Flares with RHESSI,,, *BAAS*, **35** (2), 616, 2003.
36. McConnell, M.L., Ryan, J.M., Smith, D.M., Lin, R.P., & Emslie, A.G., "RHESSI as a Hard X-Ray Polarimeter,,, *Solar Physics*, **210**, 125-142, 2002.
37. Mészáros, P., Novick, R., Chanan, G.A., Weisskopf, M.C., & Szentgyörgyi, A., "Astrophysical Implications and Observational Prospects of X-Ray Polarimetry,,, *Ap. J.*, **324**, 1056, 1988.
38. Smith, F.G., Jones, D.H.P., Dick, J.S.B., & Pike, C.D., "The Optical Polarization of the Crab Pulsar,,, *MNRAS*, **233**, 305, 1988.
39. Weiskopff, M.C., Silver, E.H., Kestenbaum, H.L., Long, K.S., & Novick, R., "A Precision Measurement of the X-Ray Polarization of the Crab Nebula without Pulsar Contamination,,, *Ap. J.*, **220**, L117, 1978.
40. Long, K.S., Chanan, G.A., & Novick, R., "The X-Ray Polarization of the Cygnus Sources,,, *Ap.J.*, **238**, 710, 1980.
41. Sunyaev, R.A., & Titarchuk, L.G., "Comptonization of Low Frequency Radiation in Accretion Disks: Angular Distribution and Polarization of Hard Radiation,,, *Astron. Astrophys.*, **143**, 374, 1985.
42. Costa, E., Cinti, M.N., Feroci, M., Matt, G., & Rapisarda, M., "Scattering Polarimetry for X-Ray Astronomy by Means of Scintillating Fibers,,, *Proc. SPIE*, **2010**, 45, 1993.
43. Feroci, M., Costa, E., Matt, G., Cinti, M.N., & Rapisarda, M., "X-Ray Scattering Polarimetry with Scintillating Fibers of Different Materials,,, *Proc. SPIE*, **2283**, 275-287, 1994.
44. Novick, R., "Stellar and Solar X-Ray Polarimetry,,, *Sp. Sci. Rev.*, **18**, 389, 1975.
45. McConnell, M., et al., "The Design of a Gamma-Ray Burst Polarimeter,,, *Compton Gamma-Ray Observatory*, ed. Friedlander et al., AIP Conf. Proc. 280, 1142, AIP, New York, 1993.
46. McConnell, M.L., et al., "Development of a Hard X-Ray Polarimeter for Solar Flares and Gamma-Ray Bursts,,, *IEEE Trans. Nucl. Sci.*, **45** (2), 910, 1998 .
47. McConnell, M.L., et al., "The Development of a Hard X-Ray Polarimeter for Gamma-Ray Bursts,,, *Gamma-Ray Bursts*, eds. C.A. Meegan, R.D. Preece, & T.M. Koshut, AIP Conf. Proc. 428, 889, AIP, New York, 1998.
48. Ryan, J.M., McConnell, M.L., Forrest, D.J., Macri, J., McClish, M., & Vestrand, W.T., "A Hard X-Ray Solar Flare Polarimeter Design Based on Scintillating Fibers,,, *SciFi97: Workshop on Scintillating Fiber Detectors*, eds. A.D. Bross, R.C. Ruchti, and M.R. Wayne, AIP Conf. Proc. 450, 586, AIP, New York, 1998.
49. McConnell, M.L., Macri, J., McClish, M., Ryan, J., Forrest, D.J. & Vestrand, W.T., "The Development of a Hard X-Ray Polarimeter for Astrophysics.,,, *IEEE Trans. Nucl. Sci.*, **46** (4), 890, 1999.
50. McConnell, M.L., Macri, M., McClish, M., & Ryan, J., "A Polarimeter for Studying Hard X-Rays from Solar Flares,,, *26th Internat. Cosmic Ray Conf.*, **6**, 21, 1999.
51. McConnell, M.L., Macri, M., McClish, M., & Ryan, J., "Recent Laboratory Tests of a Hard X-Ray Solar Flare Polarimeter,,, *Proc. SPIE*, **3764**, 70, 1999.
52. McConnell, M.L., Macri, J.R., McClish, M., & Ryan, J.M., "A Modular Hard X-Ray Polarimeter for Solar Flares,,, *High Energy Solar Physics: Anticipating HESSI*, eds. R. Ramaty and N. Mandzhavidze, ASP Conf. Ser. 206, 280, ASP, San Francisco, 2000.
53. McConnell, M.L., Ledoux, J.R. Macri, J.R. & Ryan, J.M., "A Hard X-ray Polarimeter for Gamma-Ray Bursts and Solar Flares,,, *SPIE Conf. Proc.*, **4851**, 2002.
54. Sakurai, H., Noma, M. & Niizeki, H., "A Hard X-Ray Polarimeter Utilizing Compton Scattering,,, *Proc. SPIE*, **1343**, 512, 1990.
55. McMaster, W.H. "Matrix Representation of Polarization,,, *Rev. Mod. Phys.*, **33**, 8, 1961.
56. Shah, K. et al. "$LaBr_3$:Ce Scintillators for Gamma Ray Spectroscopy,,, *IEEE Nuclear Science Symposium Conference Record*, 2002.
57. Gehrels, N., "Instrumental Background in Balloon-Borne Gamma-Ray Spectrometers and Techniques for its Reduction,,, *NIM*, **A239**, 324, 1985.
58. Paciesas, W.S., et al., "The Fourth BATSE Gamma-Ray Burst Catalog (Revised),,, *Ap. J. Supp.*, **122**, 465, 1999.
59. McConnell, M.L., et al., "Gamma-Ray Observations of the Crab Region Using a Coded-Aperture Telescope,,, *Ap. J.*, **321**, 543, 1987.
60. McConnell, M.L., et al., "Gamma-Ray Observations of Cygnus X-1 and Cygnus X-3 Using a Coded-Aperture Telescope,,, *Ap. J.*, **343**, 317, 1989.
61. Dunphy, P.P., et al., "A Balloon-Borne Coded Aperture Telescope for Low-Energy Gamma-Ray Astronomy,,, *NIM*, **A274**, 362, 1989.